

High Frequency Modal Identification on Noisy High-Speed Camera Data

Jaka Javh^a, Janko Slavič^{a,*}, Miha Boltežar^a

^a*University of Ljubljana, Faculty of Mechanical Engineering, Aškerčeva 6, 1000 Ljubljana, Slovenia*

Cite as:

Jaka Javh, Janko Slavič, Miha Boltežar
High Frequency Modal Identification on Noisy High-Speed Camera Data
Mechanical Systems and Signal Processing, Vol. 98, p. 344-351, 2018
DOI: 10.1016/j.ymsp.2017.05.008

Abstract

Vibration measurements using optical full-field systems based on high-speed footage are typically heavily burdened by noise, as the displacement amplitudes of the vibrating structures are often very small (in the range of micrometers, depending on the structure). The modal information is troublesome to measure as the structure's response is close to, or below, the noise level of the camera-based measurement system. This paper demonstrates modal parameter identification for such noisy measurements. It is shown that by using the Least-Squares Complex-Frequency method combined with the Least-Squares Frequency-Domain method, identification at high-frequencies is still possible. By additionally incorporating a more precise sensor to identify the eigenvalues, a hybrid accelerometer / high-speed camera mode shape identification is possible even below the noise floor. An accelerometer measurement is used to identify the eigenvalues, while the camera measurement is used to produce the full-field mode shapes close to 10 kHz. The identified modal parameters improve the quality of the measured modal data and serve as a reduced model of the structure's dynamics.

*Corresponding author

Email address: `janko.slavic@fs.uni-lj.si` (Janko Slavič)

Keywords: mode shape, high-speed camera, modal parameter identification, noise, optical flow, LSCF, Experimental Modal Analysis

1. Introduction

True full-field mode shapes are hard to measure. Measurements using accelerometers produce sparse spatial information [1], laser vibrometers need to scan the surface and do not produce an instantaneous measurement [2, 3] and interferometric techniques such as Electronic Speckle Pattern Interferometry [4] measure the out-of-plane displacements, only. Displacement measurements using high-speed cameras are increasingly being used in modal analysis, because they can produce a dense, simultaneous, full-field 3D measurement [5, 6]. The displacements can be identified from image sequences with methods such as Digital Image Correlation [7], Gradient-based Optical Flow [8–10], Point Tracking [11] and Phase-based methods [12].

Optical measurements using cameras have been used in civil engineering, where the displacement response at lower frequencies (below 100 Hz) is relatively large [13–18]. Measurements with dynamic responses up to approximately 1 kHz have also been demonstrated in [3, 19–23] with some spanning up to about 2 kHz [24–26] and at most up to 2.4 kHz [10, 27]; however, frequencies above 1 kHz are problematic because the displacement response is generally less than micrometers, depending on the structure [10, 24]. Such small displacements are significantly below the camera’s pixel size and therefore produce signals which are at, or below, the camera noise floor, making them appear unidentifiable.

Modal identification returns the modal parameters from the measurements. These modal parameters are usually in the form of a modal model [28], which comprises the natural frequencies and damping (eigenvalues) and the mode shapes (modal constants). Among the large number of modal-parameter identification methods the LSCF (Least-Squares Complex Frequency) [29] in combination with the LSFD (Least-Squares Frequency Domain) [30] is the most commonly used, because it is fast and robust [31].

Perhaps the first modal identification performed on camera measurements was performed by NASA on the MIR space station, where they used the Eigenvalue Realization Algorithm [18]. Modal identification has also been performed on optical measurements by implementing motion magnification and edge detection to produce mode shapes [22]. In [32] the authors used

modal parameter identification to determine mode shapes for damage detection. The authors of [33] compared the mode shapes measured by Digital Image Correlation, 3D Point-Tracking, 3D Laser Vibrometry, and accelerometer measurements. Among others, papers [34, 35] demonstrate the operational modal analysis using camera systems. Modal identification has also been used as a concept for building-structure health monitoring [14].

The above mentioned papers are examples of lower-frequency vibrations (range of tens to hundreds of Hz) with relatively larger displacements. The goal of this research is to identify the modal information up to 10 kHz, where the camera noise prevails. The identification is expected to improve the quality of the measured data and increase the range of use for high-speed camera systems in modal analysis. The widely accepted LSCF/LSFD method is used on a hybrid measurement combining a precise accelerometer and a full-field displacement response identified from a high-speed camera measurement using a simplified Gradient-based Optical Flow [10]. The accelerometer measurement is used to produce reliable eigenvalue identification using LSCF and these eigenvalues are then used in the LSFD mode shape identification on the full-field camera measurement.

The text is organized as follows: Section 2 covers an overview of the Gradient-based Optical Flow used to identify the motion from videos, followed by an overview of the LSCF/LSFD modal-parameter-identification techniques. Section 3 combines the motion identification and modal parameter identification in an analysis of a lab-scale experiment, demonstrating modal parameter identification at high frequencies and with high levels of noise.

2. Theoretical background

2.1. Gradient-based Optical Flow

To identify the motion from an image sequence, a simplified Gradient-based Optical Flow (SGBOF) [10] was used in this research. The method is based on a linear relation between the change in intensity of pixels (or subsets of pixels) $I(x, y, t)$ and the displacements Δs . Displacements Δs are obtained as the change in intensity over time divided by the intensity gradient ∇I :

$$\Delta s = \frac{I(x, y, t) - I(x, y, t + \Delta t)}{|\nabla I|} \quad (1)$$

Variables x and y are the discrete pixel locations and t is time. The SGBOF method produces the most direct route from the optical information to the displacement. The intensity gradient $|\nabla I|$ is determined by the numerical derivation of a reference image. From Equation (1) it is clear that the sensitivity to displacement is best where the intensity gradient is highest and that the displacement Δs of a pixel can only be determined in the direction of the image gradient. The displacements in 2D can be measured by filming a speckle pattern and using a subset of pixels to produce an estimate of the motion and 3D measurements can be performed using a stereoscopic set-up.

2.2. Modal parameter identification

A common viscously damped model for a structure's dynamic response is formulated with partial fractions as:

$$\alpha_{jk}(\omega) = \sum_{r=1}^N \left(\frac{{}_r A_{jk}}{i\omega - \lambda_r} + \frac{{}_r A_{jk}^*}{i\omega - \lambda_r^*} \right), \quad (2)$$

where $\alpha_{jk}(\omega)$ is the displacement frequency-response function (receptance) of a response point j to an excitation at point k , λ_r are the system eigenvalues containing the angular eigenfrequencies ω_r and the damping ratios ζ_r according to:

$$\lambda_r = -\zeta_r \omega_r \pm i \omega_r \sqrt{1 - \zeta_r^2} \quad (3)$$

and ${}_r A_{jk}$ are the modal constants, which result in the mode shapes. The formulation (2) indicates the modal decomposition, where the response equals the sum of the modes ($\lambda_r, {}_r A_{jk}$) and their complex conjugates ($\lambda_r^*, {}_r A_{jk}^*$). The purpose of modal-parameter-identification techniques is to identify the modal parameters ($\lambda_r, {}_r A_{jk}$) from measurements of a structure's response.

One such identification technique is the Least-Squares Complex Frequency (LSCF) method. LSCF is a frequency-domain method derived from a common-denominator receptance model [29]:

$$\alpha_j(\omega) = \frac{\sum_{r=0}^{2N} a_{j,r} e^{-i r \Delta t \omega}}{\sum_{r=0}^{2N} b_r e^{-i r \Delta t \omega}} \quad (4)$$

Index k is omitted, because the excitation should be the same for all the measured responses (a Single-Input Multiple-Output measurement).

In the common-denominator model the values b_r governing the eigenvalues λ_r of the system are the same for each response location j . A least-squares criterion is used to produce a system of equations [29]:

$$\left(\sum_{j=1}^p [O_j] - [S_j]^T [R_j]^{-1} [S_j] \right) \{b\} = [\Lambda] \{b\} = 0, \quad (5)$$

where $\{b\}$ is the vector of the denominator coefficients $\{b_0, b_1, \dots, b_{2N}\}^T$.

The matrices $[O_j]$, $[S_j]$, $[R_j]$ are of a Toeplitz structure of shape $(2N+1 \times 2N+1)$. A Toeplitz matrix has repetitive elements, which can be determined once, reducing the computation. The elements (l - row, c - column, $n = 1, 2, \dots, L$ - frequency points) are determined by [29]:

$$R_{j,lc} = \sum_{n=1}^L \left(|W_j(\Omega_n)|^2 e^{2\pi i (l-c) n L} \right) \quad (6)$$

$$S_{j,lc} = - \sum_{n=1}^L \left(|W_j(\Omega_n)|^2 H_j(\Omega_n) e^{2\pi i (l-c) n L} \right) \quad (7)$$

$$O_{j,lc} = \sum_{n=1}^L \left(|W_j(\Omega_n) H_j(\Omega_n)|^2 e^{2\pi i (l-c) n L} \right) \quad (8)$$

The relations (6)-(8) are in fact the Discrete Fourier Transforms of the functions $|W_j(\Omega_n)|^2$, $|W_j(\Omega_n)|^2 H_j(\Omega_n)$ and $|W_j(\Omega_n) H_j(\Omega_n)|^2$; therefore, the Fast Fourier algorithm can be used for a fast calculation [29]. $W_j(\omega)$ are the weighting functions for each response location. The coherence can be used as a weighting function; however, as only one measurement was taken, the coherence was not obtained, also to reduce the computational cost no weighting function was used ($W_j(\Omega_n) = 1$ for all j and n). Without the weighting function the matrices $[R_j]$ reduce to the identity matrix, greatly simplifying the calculation of the sum in equation (5).

By imposing $b_{2N} = 1$, thereby removing the parameter redundancy, system (5) reduces to a shape of $(2N \times 2N)$ and can be solved via the inverse to produce vector $\{b\}$ and therefore the coefficients b_r that determine the identified eigenvalues as roots of the denominator polynomial.

An identification order N higher than the number of modes is typically used to accommodate the noise and other errors as fictitious/numerical poles. A well-known procedure for identifying true eigenvalues is to repeat the identification for increasing orders of identification and then hand picking the

true eigenvalues from stabilization diagrams based on whether the identified values are converging over the increasing modal estimation order N . The picked eigenvalues are then used to determine the numerator coefficients $a_{j,r}$ for every response location j separately.

The numerator coefficients $a_{j,r}$ in Equation (4), and consequently the modal constants ${}_r A_j$, can be determined in the next step using the LSCF; however, because of a poor identification, the Least-Squares Frequency-Domain method (LSFD) is typically used instead [36]. After the eigenvalues of the system are determined, the modal constants can be determined by using the LSFD method, based on the model:

$$\alpha_j(\omega) = \sum_{r=1}^N \left(\frac{{}_r A_j}{i\omega - \lambda_r} + \frac{{}_r A_j^*}{i\omega - \lambda_r^*} \right) - \frac{A_L}{\omega^2} + A_U, \quad (9)$$

where the variables A_L and A_U are the lower and upper residuals, compensating for the modes above and below the measured frequency range. The modal constants are obtained by constructing a linear set of equations (9) for all the frequency points $\Omega_1, \Omega_2, \dots, \Omega_L$, producing an overdetermined system. The solution is obtained by solving a pseudo-inverse.

3. Modal parameter identification on Optical Flow data

Displacement measurements using cameras produce a dense full-field of responses; however, the combination of high levels of noise and small displacements at higher frequencies, produces measurements less accurate than an accelerometer or a laser vibrometer. The displacements caused by vibrations tend to fall below the level of noise, making it seem as though the response cannot be identified; however, the vibration signal is still present, only that it is masked by noise. The modal identification of data below the noise floor is predicted to be still possible, because modern identification techniques such as the LSCF/LSFD incorporate the response of a wider frequency range in the least-squares solution, thereby decreasing the effect of noise on the identified parameters.

The modal identification was tested on real world data.

3.1. The measurement

A measurement of a solid steel beam with dimensions $15 \times 30 \times 500$ mm was performed in approximately free-free conditions. The beam was chosen

because its response is well known and the results can be easily evaluated. A B&K 4508 B001 accelerometer was attached at one side of the beam and a PCB 086C03 modal hammer was used to excite the beam. The hammer impact was in line with the ropes, to produce smaller rigid-body displacements. The response was measured with a Fastcam SA-Z high-speed camera. A sticker with black and white lines was applied to the beam to make the displacements more evident to the camera. The camera filmed the thinner side of the beam, thereby measuring the bending of the beam (Figure 2). The camera filmed at 200,000 fps at a resolution of 1024×64 pixels and captured 698.984 frames (a sampling period of ~ 3.5 s), producing 64 GB of data. The displacements were identified at 7521 points on the beam. The accelerometer and the modal hammer-force sensor were sampled using a NI9233 card with 50,000 Hz for a sampling period matching that of the camera to produce the same frequency resolution. A hard metal tip was used on the modal hammer and the hit was of considerable force (impulse length of ~ 0.14 ms, peaking at 2.6 kN) for the higher frequencies to be made visible.

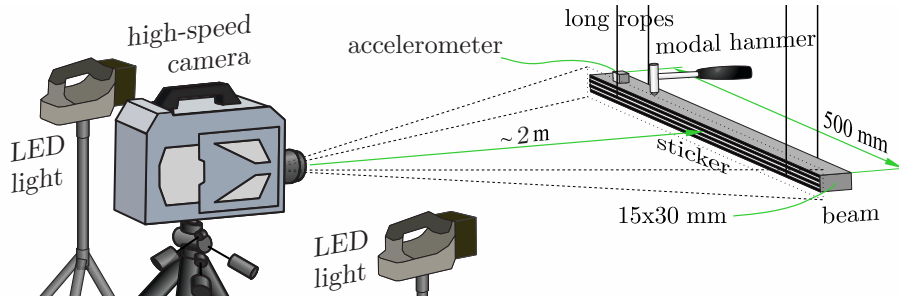


Figure 1: The schematic of the measurement set-up

3.2. Identification of eigenvalues

First an attempt was made at identifying the eigenvalues from the camera measurement. Due to the high levels of noise and the large frequency range (0–9500 Hz) a high order of identification ($N=500$) was used to produce more apparent stabilization diagrams. The spectrum was measured up to 100 kHz, but only the range up to 9500 Hz was used for the parameter identification, because the first lobe of the hammer-impulse force spectrum ranged only up to 10 kHz. A high sampling rate was used to capture a larger number of samples for the impact transient response, improving the signal-to-noise ratio [37]. A slight time shift had to be imposed on the camera measurement,



Figure 2: A photograph of the measurement set-up

due to the apparent trigger differences. The stabilization diagram for the camera measurement using the LSCF was performed (Figure 3).

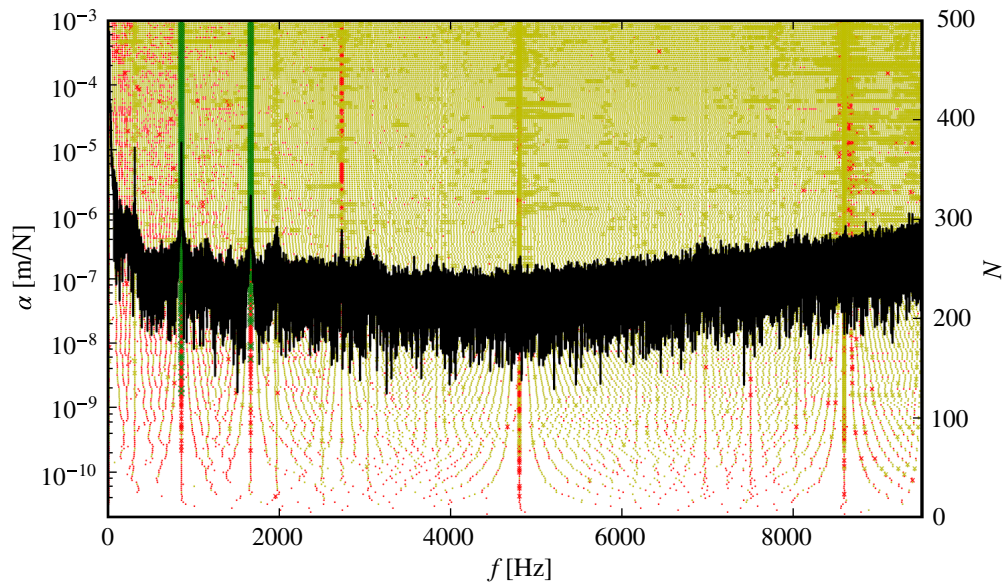


Figure 3: The stabilization diagram for the camera measurement using LSCF

Only eigenvalues up to the third mode at ~ 2730 Hz are identified and some of these modes are identified as unstable. The higher modes seem to be masked under the camera noise level, which is at 0.00035 pixel (determined as the standard deviation of a flat noisy range of the camera measurement

spectrum). Due to the poor eigenvalue identification from the camera measurements, the accelerometer data was used to identify the eigenvalues (Figure 4) and the camera measurements to identify the modal constants of the full-field in the following step.

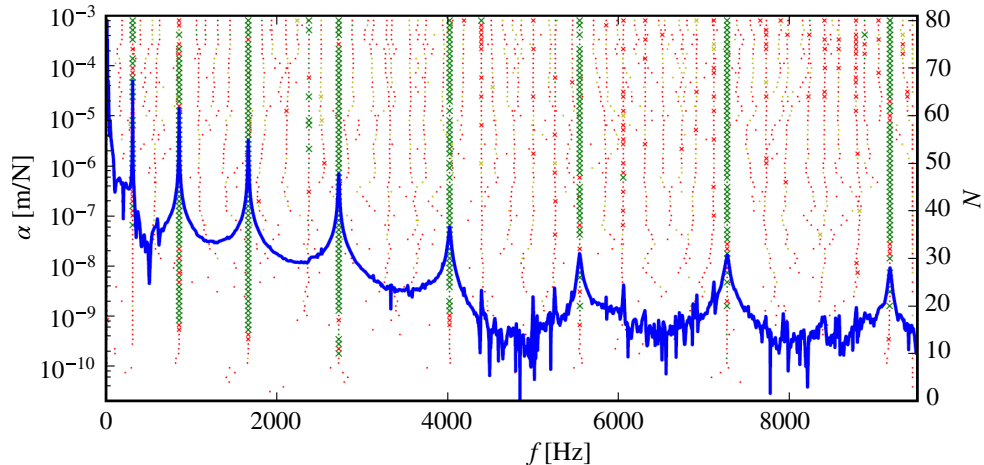


Figure 4: The stabilization diagram for the accelerometer measurement using LSCF

3.3. Identification of mode shapes

The accelerometer eigenvalues up to the 8th mode at 9 kHz were used in the identification of the modal constants from the camera measurement in the hope of identifying the response below the camera's noise floor.

The full-field camera measurement produced up to eight response points over the beam's thickness; these points are situated at the same beam length and were averaged to improve the signal-to-noise ratio.

Simply by plotting the amplitudes of the spectra measured by the camera α_j for the frequencies \tilde{f}_r closest to the identified eigenfrequencies f_r produces the indicated mode shapes (Figure 5). The modes above the 4th mode are not, or are barely, recognizable. The mode shapes identified with the LSCF are expected to be clearer, because they incorporate the surrounding frequencies in the identification; therefore, the influence of the noise is expected to be smaller.

There were apparent problems with the two rigid-body modes and the first bending mode. The rigid-body response seems to be nonlinear, resulting from the rope's nonlinear stiffness, and cannot be identified properly. This is

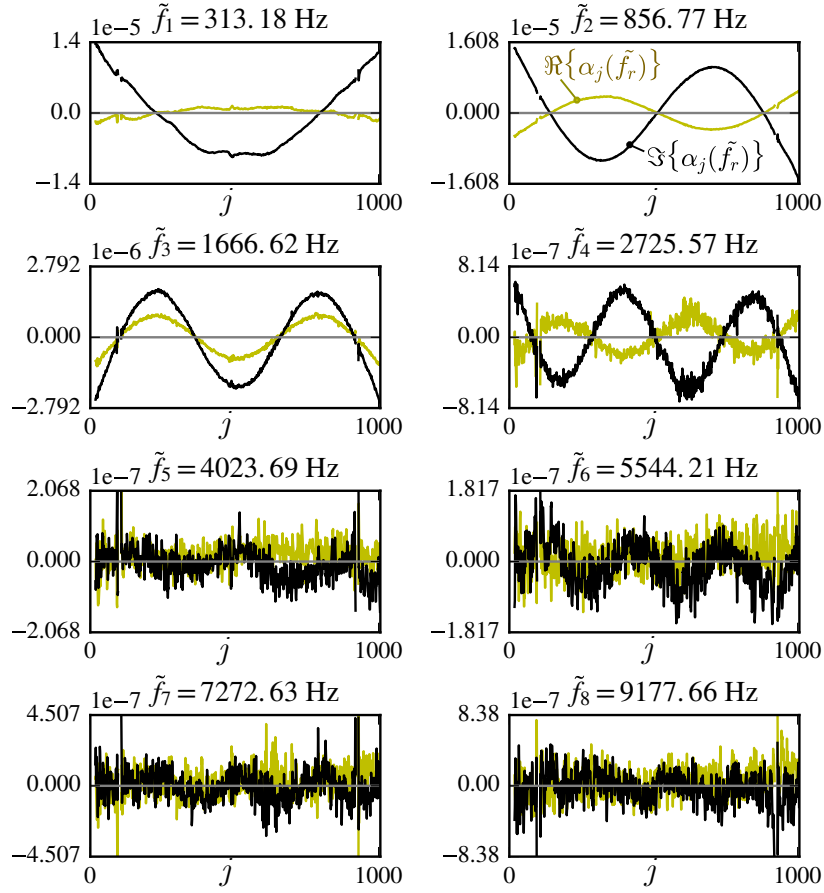


Figure 5: The amplitudes of the camera measured spectra $\alpha_j(\tilde{f}_r)$ over the beam's length for the frequencies closest to the eigenfrequencies $\tilde{f}_{1,2,3,\dots}$. The plots indicate the beam's mode shapes only up to the fourth mode

why the lower spectrum (up to 300 Hz) was omitted from the LSFD modal constants identification. The modal constants, producing the mode shapes, are shown in Figure 6. The first 8th bending mode shapes of the beam are identified and correspond to the well-known beam mode shapes.

3.4. Reconstruction

The identified modal parameters can be used to reconstruct the identified receptance. The identified receptance curve for a point below the accelerometer is shown in Figure 7 along with the receptance measured by the accelerometer and the receptance measured by the camera. The identified receptance is

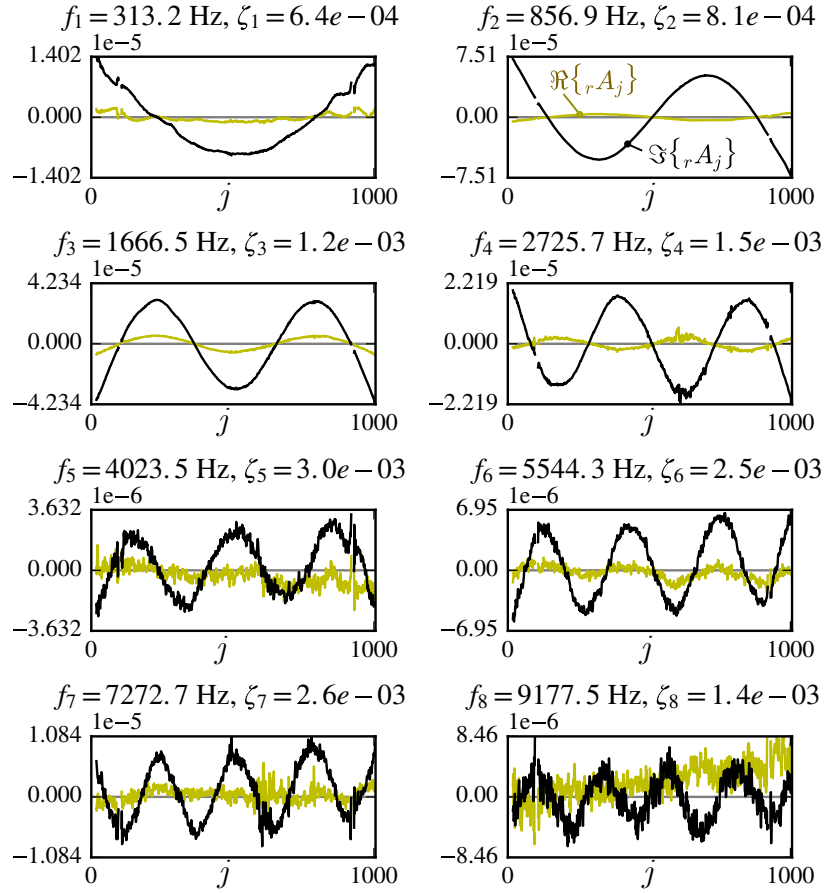


Figure 6: The beam’s modal constants identified with LSFD from the camera measurement using the eigenvalues determined from the accelerometer measurement. The modal constants are plotted over the beam’s length and display the first eight measured beam’s mode shapes close to 10 kHz

produced from the eigenvalues identified from the accelerometer receptance and the modal constants from the camera measurement. This combination enabled the identification of full-field high-frequency mode shapes close to 10 kHz (Figure 6), despite the fact that the resonant peaks are below the noise level of the camera measurement, proving that the modal information is present and can be extracted from very noisy measurements.

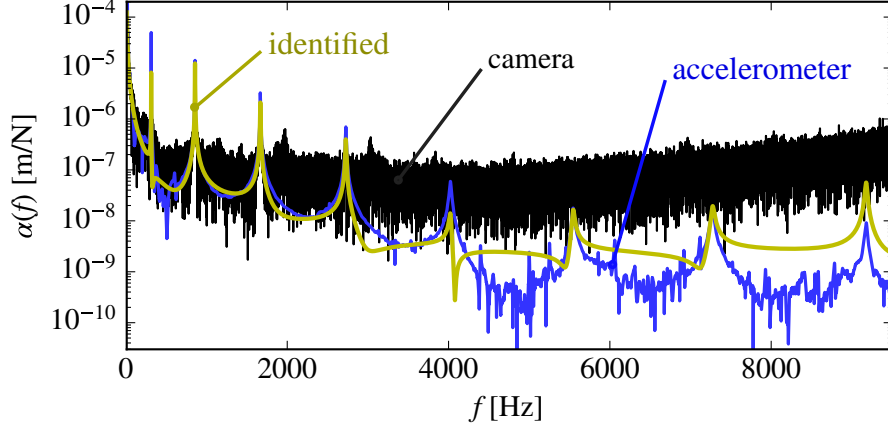


Figure 7: The reconstructed receptance using the accelerometer eigenvalues and the camera modal constants for a point below the accelerometer

3.5. Computation time

Full-field measurements produce large amounts of data, weighing heavily on the computation time. This section is meant to give some idea of the computational burden.

The simplified Gradient-based Optical Flow analysis of the 64 GB of data requires only about 2.5 minutes on 16 processor cores.

Limiting to 7521 response points and by cutting the frequency range to 0–9500 Hz reduced the amount of data to 3 GB of complex spectra.

The LSCF eigenvalue identification for the stabilization diagram in Figure 3 required 4 h and 20 min, mainly due to the calculation of the sum from Equation (5) (single processor core). In comparison, the stabilization for the accelerometer measurement in Figure 4 required only 3 seconds to compute.

The calculation of the modal constants is not demanding, because the pseudo-inverse can be calculated only once and is the same for all the response locations j . The modal constants in Figure 6 were computed in 7 seconds.

The end results were produced from the accelerometer measured eigenvalues and the modal constants measured by the camera, therefore the combined identification required only approximately 10 s to compute.

4. Conclusion

This research analyses the modal parameter identification on full-field displacement measurements obtained with a high-speed camera. The displacement time series measured by the camera are very noisy, due to the displacements being so small. To identify the modal parameters, over-determined least-squares solutions are used. The identification is performed using LSCF/LSFD. Using the camera measurements, only the first four beam modes were identified; however, by additionally using the eigenvalues from the more precise accelerometer measurement, the mode shapes close to 10 kHz were identified from the camera measurements, despite being below the noise floor. The combination of the accelerometer (or any other appropriate sensor) and the camera combines the best of both worlds; a single precise sensor (e.g. accelerometer) produces precise eigenvalues and the camera produces the full-field mode shapes.

In future work, weighting functions could be used, particularly in the identification of the eigenvalues, to improve the stabilization diagram of the camera measurement in Figure 3 and produce more precise values. Also, producing multiple measurements and averaging them is a viable option to improving the data, however, as transferring the 64 GB of data from the camera to the PC takes approx. 30 minutes, this approach is not often used.

Acknowledgment

The authors acknowledge the partial financial support from the Slovenian Research Agency (research core funding No. P2-0263 and J2-6763).

References

- [1] C. Schedlinski, J. Schell, E. Biegler, J. Sauer, Application of optical measurement techniques for experimental modal analyses of lightweight structures, *Proceedings of ISMA2016* (2016) 2301–2314.
- [2] A. B. Stanbridge, D. J. Ewins, Modal testing using a scanning laser doppler vibrometer, *Mechanical Systems and Signal Processing* 13 (2) (1999) 255–270.

- [3] D. A. Ehrhardt, M. S. Allen, S. Yang, T. J. Beberniss, Full-field linear and nonlinear measurements using continuous-scan laser doppler vibrometry and high speed three-dimensional digital image correlation, *Mechanical Systems and Signal Processing* 86 (2017) 82–97.
- [4] O. Lekberg, Electronic speckle pattern interferometry, *Physics in technology* 11 (1) (1980) .
- [5] M. N. Helfrick, C. Niezrecki, P. Avitabile, T. Schmidt, 3D digital image correlation methods for full-field vibration measurement, *Mechanical Systems and Signal Processing* 25 (2011) 917–927.
- [6] J. Baqersad, P. Poozesh, C. Niezrecki, P. Avitabile, Photogrammetry and optical methods in structural dynamics - a review, *Mechanical Systems and Signal Processing* 86 (2017) 17–34.
- [7] W. Peters, W. Ranson, Digital imaging techniques in experimental stress analysis, *Optical Engineering* 21 (3) (1982) 427–431.
- [8] B. Lucas, T. Kanade, An iterative image registration technique with an application to stereo vision, *International Joint Conference on Artificial Intelligence* (1981) 674–679.
- [9] B. Horn, B. Schunck, Determining optical flow, *Technical Symposium East. International Society for Optics and Photonics* (1981) 319–331.
- [10] J. Javh, J. Slavič, M. Boltežar, The subpixel resolution of optical-flow-based modal analysis, *Mechanical Systems and Signal Processing* 88 (2017) 89–99.
- [11] P. Olaszek, Investigation of the dynamic characteristic of bridge structures using a computer vision method, *Measurement* 25 (3) (1999) 227–236.
- [12] D. J. Fleet, A. D. Jepson, Computation of component image velocity from local phase information, *International journal of computer vision* 5 (1) (1990) 77–104.
- [13] E. Caetano, S. Silva, J. Bateira, Vision system for vibration monitoring of civil engineering structures, *Experimental Techniques* 35 (4) (2011) 74–82.

- [14] B. K. Oh, J. W. Hwang, Y. Kim, T. Cho, H. S. Park, Vision-based system identification technique for building structures using a motion capture system, *Journal of Sound and Vibration* 356 (2015) 72–85.
- [15] J. Guo, C. Zhu, Dynamic displacement measurement of large-scale structures based on the lucaskanade template tracking algorithm, *Mechanical Systems and Signal Processing* 66 (2016) 425–436.
- [16] B. Pan, L. Tian, X. Song, Real-time, non-contact and targtless measurement of vertical deflection of bridges using off-axis digital image correlation, *NDT&E International* 79 (2016) 73–80.
- [17] P. Poozesh, J. Baqersad, C. Niezrecki, P. Avitabile, E. Harvey, R. Yarala, Large-area photogrammetry based testing of wind turbine blades, *Mechanical Systems and Signal Processing* 86 (2017) 98–115.
- [18] M. Gilbert, S. Welch, STS-74/MIR photogrammetric appendage structural dynamics experiment, *Proceedings of the 1996 37th AIAA/ASME/ASCE/AHS/ASC Structures Structural Dynamics and Materials Conference* (1996) 1594–1604.
- [19] T. Siebert, R. Wood, K. Splitthof, High speed image correlation for vibration analysis, *Journal of Physics* 181 (1) (2009) .
- [20] W. Wang, J. E. Mottershead, A. Ihle, T. Siebert, H. R. Schubach, Finite element model updating from full-field vibration measurement using digital image correlation, *Journal of Sound and Vibration* 330 (8) (2011) 1599–1620.
- [21] A. Davis, J. G. Chen, F. Durand, Image-space modal bases for plausible manipulation of objects in video, *ACM Transactions on Graphics (TOG) - Proceedings of ACM* 34 (6) (2015) .
- [22] Y. Yang, C. Dorn, T. Mancini, Z. Talken, G. Kenyon, C. Farrar, D. Mascarenas, Blind identification of full-field vibration modes from video measurements with phase-based video motion magnification, *Mechanical Systems and Signal Processing* 85 (2017) 567–590.
- [23] S. Zhong, J. Zhong, Q. Zhang, N. Maia, Quasi-optical coherence vibration tomography technique for damage detection in beam-like structures

based on auxiliary mass induced frequency shift, *Mechanical Systems and Signal Processing* 93 (2017) 241–254.

- [24] T. J. Beberniss, D. A. Ehrhardt, High-speed 3D digital image correlation vibration measurement: Recent advancements and noted limitations, *Mechanical Systems and Signal Processing* 86 (2017) 35–48.
- [25] P. L. Reu, D. P. Rohe, L. D. Jacobs, Comparison of DIC and LDV for practical vibration and modal measurements, *Mechanical Systems and Signal Processing* 86 (2017) 2–16.
- [26] R. Perez, G. Bartram, T. Beberniss, R. Wiebe, S. M. Spottswood, Calibration of aero-structural reduced order models using full-field experimental measurements, *Mechanical Systems and Signal Processing* 86 (2017) 49–65.
- [27] J. G. Chen, N. Wadhwa, Y. J. Cha, F. Duran, T. Freeman, O. Buyukozturk, Modal identification of simple structures with high-speed video using motion magnification, *Journal of Sound and Vibration* 345 (2015) 58–71.
- [28] D. J. Ewins, *Modal Testing: Theory and Practice*, John Wiley & Sons, Ontario, Canada, 1984.
- [29] P. Guillaume, P. Verboven, S. Vanlanduit, Frequency-domain maximum likelihood identification of modal parameters with confidence intervals, *Proceedings of ISMA* 23 (1998) 16–18.
- [30] H. V. Auweraer, W. Leurs, P. Mas, L. Hermans, Modal parameter estimation from inconsistent data sets, *Proceeding of IMAC XVIII* (2000) 763–771.
- [31] B. Peeters, H. Van der Auweraer, P. Guillaume, J. Leuridan, The poly-MAX frequency-domain method: A new standard for modal parameter estimation?, *Shock and Vibration* 11 (3-4) (2004) 395–409.
- [32] U. P. Poudel, G. Fu, J. Ye, Structural damage detection using digital video imaging technique and wavelet transformation, *Journal of Sound and Vibration* 286 (4) (2005) 869–895.

- [33] C. Warren, C. Niezrecki, P. Avitabile, P. Pingle, Comparison of FRF measurements and mode shapes determined using optically image based, laser, and accelerometer measurements, *Mechanical Systems and Signal Processing* 25 (6) (2011) 2191–2202.
- [34] J. Baqersad, J. Carr, T. Lundstrom, C. Niezrecki, P. Avitabile, M. Slatery, Dynamic characteristics of a wind turbine blade using 3D digital image correlation, *SPIE Smart Structures and Materials+ Nondestructive Evaluation and Health Monitoring* (2012) 83482I–83482I.
- [35] C. Van Karsen, T. Bouman, G. Gwaltney, Operating deflection shapes of a violin string via high speed/high resolution videography, *Topics in Modal Analysis* 7 (2014) 637–644.
- [36] B. Cauberghe, Applied frequency-domain system identification in the field of experimental and operational modal analysis, Ph.D. thesis, Vrije Universiteit Brussel (2004).
- [37] J. Tsui, Digital techniques for wideband receivers, SciTech Publishing, Raleigh, 2004.